Bidirectional Beam Propagation Method Based on Axi-Symmetric Full-Vectorial Finite Element Method

Bidirectional Beam Propagation Method Based on Axi-symmetric Full-Vectorial Finite Element Method

Akito Iguchi, *Member, IEEE,* Keita Morimoto, *Graduate Student Member, IEEE,*
and Yasuhide Tsuji, *Senior Member, IEEE*

Abstract—We first present a bidirectional beam propagation method (BiBPM) based on axially symmetric full-vectorial finite element method (Axi-FVFEM). The Axi-FVFEM based BiBPM is a more versatile method than previous scalar BiBPM for axi-symmetric structure. It has potential to offer more efficient analysis than widely used FEM or finite difference based techniques, especially for a large scale waveguide such as a long periodic structure. An air gap in an axi-symmetric waveguide and a fibre Bragg grating (FBG) are analyzed using the Axi-FVFEM based BiBPM for numerical validation, and we compare the numerical results with those of a 3D finite-difference time-domain (FDTD) method and a modal-based method.

Index Terms—bidirectional beam propagation method, full vectorial finite element method, axially symmetric waveguide.

I. INTRODUCTION

AS an analysis and design tool of axially symmetric optical components, an axi-symmetric 2D finite element method (Axi-2DFEM) [1], or a body of revolution finite difference time-domain(BOR-FDTD) [2], [3] method are widely employed. However, it is well known that massive computational effort is required when an optical waveguide which is much larger than operating wavelength is directly modeled by the FEM or the FDTD. Field-based methods such as bidirectional beam propagation methods (BiBPMs) and modal-based methods, also known as mode matching methods (MMMs), have been well investigated to analyze longitudinally multilayered waveguides efficiently and wide variety of variants have been developed so far [4]–[11]. Modal-based methods for axi-symmetric waveguides have already been reported [8] and been used as a numerical validation tool [12], however in general, sufficient large number of eigenpairs, which are time consuming to compute, are necessary for accurate analysis. Field-based methods have advantage that all eigenmodes containing continuous modes are taken into account without calculation of eigenpairs by computing accurately a square root of characteristic matrix $\sqrt{[Q]}$ [10], [11]. Moreover, investigation of dominant eigenmodes and sufficient mode number are not necessary unlike the modal-based methods. Recently, a BiBPM based on scalar axi-symmetric FEM is
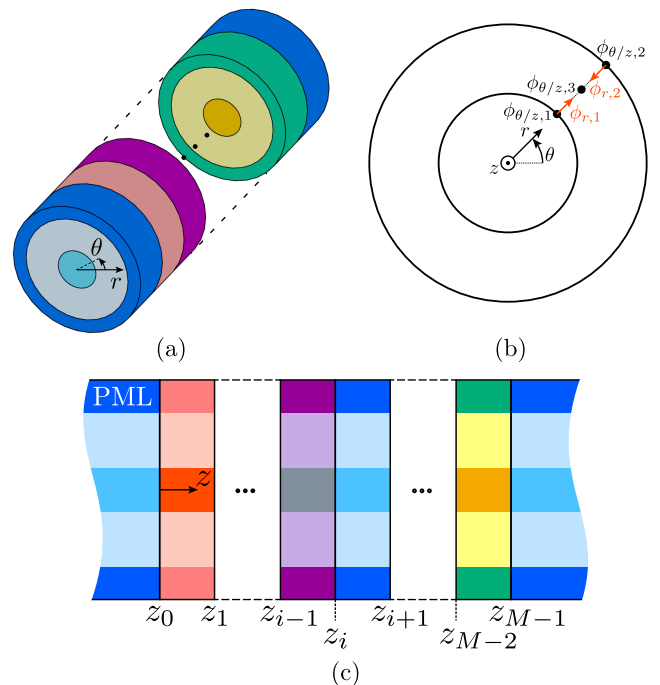
Fig. 1. An axially symmetric optical waveguide. (a) 3D view of an axi-symmetric waveguide. (b) A ringed edge element used in this letter. (c) A schematic of a axi-symmetric multi-layered waveguide.

reported, and its effectiveness is investigated comparing with the Axi-2DFEM and the FDTD methods [13]. In this literature, $\sqrt{[Q]}$ is treated accurately and efficiently using a blocked version Schur decomposition (B-Schur) [14] with a branch-cut technique. Its full-vectorial version is desirable to treat optical waveguides correctly, in particular high-index-contrast waveguides, or optical components with sensitive properties to effective index.

In this letter, we first present a BiBPM based on full-vectorial finite element method (Axi-FVFEM) to deal with various axi-symmetric waveguides. For numerical validation, an air-gap in dielectric circular waveguide surrounded by air and a fibre Bragg grating (FBG) [12] are analyzed using the present method with comparing the results of other numerical modeling.

II. FORMULATION

We consider axi-symmetric waveguide, and computational window is terminated by a perfectly matched layer (PML) [15] as shown in Fig. 1(a). The wave equation in this system is derived from Maxwell's equation as follows:

$$\nabla \times \left([p] \nabla \times \boldsymbol{\Phi}\right) - k_0^2 [q] \boldsymbol{\Phi} = \mathbf{0} \tag{1}$$

$$[p] = \left\{ \begin{array}{l} [\mu]_{\text{PML}}^{-1} \\ [\varepsilon]_{\text{PML}}^{-1} \end{array} \right., \quad [q] = \left\{ \begin{array}{ll} [\varepsilon]_{\text{PML}} & (\boldsymbol{\Phi} = \sqrt{\varepsilon_0} [s] \boldsymbol{E}) \\ [\mu]_{\text{PML}} & (\boldsymbol{\Phi} = \sqrt{\mu_0} [s] \boldsymbol{H}) \end{array} \right.$$

$$[\varepsilon]_{\text{PML}} = \det\left([s]\right) [s]^{-1} [\varepsilon_r] [s]^{-1}$$
$$[\mu]_{\text{PML}} = \det\left([s]\right) [s]^{-1} [\mu_r] [s]^{-1}$$

where k_0 is a wavenumber in vacuum, $[\varepsilon_r]$ and $[\mu_r]$ are relative permittivity and permeability tensors. For simplification, we let these tensors diagonal matrices, i.e. $[p] = \text{diag}\,\{p_r, p_\theta, p_z\}$, $[q] = \text{diag}\,\{q_r, q_\theta, q_z\}$. $[s]$ is related to a stretching parameter of the PML in cylindrical coordinate.

$$[s] = \begin{bmatrix} s & 0 & 0 \\ 0 & s' & 0 \\ 0 & 0 & 1 \end{bmatrix}$$

$$s(r) = \left\{ \begin{array}{ll} 1 & [0 \le r < r_{\text{PML}}] \\ 1 - j\alpha \left(\frac{r - r_{\text{PML}}}{L_r - r_{\text{PML}}}\right)^M & [r_{\text{PML}} \le r \le L_r] \end{array} \right.$$

$$s'(r) = \frac{1}{r} \int_0^r s(R) dR.$$

α is a loss tangent, L_r is size of computational window including the PML, and $(L_r - r_{\text{PML}})$ indicates the thickness of the PML. First, we assume the EM wave has a phase factor of $\exp(-j\beta z - jm\theta)$. The functional in this system can be written as follows when $\boldsymbol{\Phi} = \mathbf{0}$ at terminal boundary of the computational window (Ω).

$$F = \iint_\Omega \left\{ (\nabla \times \boldsymbol{\Phi})^* \cdot \left([p] \nabla \times \boldsymbol{\Phi}\right) - k_0^2 [q] \boldsymbol{\Phi}^* \cdot \boldsymbol{\Phi} \right\} d\Omega \tag{2}$$

where $*$ indicates complex conjugate.

It is known that in full-vectorial FE analysis nonphysical spurious modes are eliminated by using hybrid edge/nodal elements [16]. We expand the electro-magnetic (EM) field in a local element using the cylindrical ringed edge element shown in Fig. 1(b):

$$\boldsymbol{\Phi}_e = [N]^T \{\phi\}_e \exp\left(-j\beta z - jm\theta\right) \tag{3}$$

$$[N] = \begin{bmatrix} \{M\} & \{0\} & \{0\} \\ \{0\} & j\{N\} & \{0\} \\ \{0\} & \{0\} & j\{N\} \end{bmatrix}, \quad \{\phi\}_e = \left\{ \begin{array}{l} \{\phi\}_{r,e} \\ \{\phi\}_{\theta,e} \\ \{\phi\}_{z,e} \end{array} \right\}$$

where ^{T} indicates transpose, the subscript "e" indicates quantity in a local domain, $\{M\}$ and $\{N\}$ are vectors of the shape function for r and θ, z direction, respectively. By applying (3) and the variational principle to (2), the following eigenvalue equation can be derived.

$$[Q] \{\phi\}_t - \beta^2 \{\phi\}_t = \{0\} \tag{4}$$

where $\{\phi\}_t = \{\{\phi\}_r, \{\phi\}_\theta\}^T$. $[Q]$ is the characteristic matrix which can be written by

$$[Q] = \left([B]_{tz} [A]_{zz}^{-1} [B]_{zt} - [C]_{tt}\right)^{-1} [A]_{tt} \tag{5}$$

$$[A]_{tt} = \begin{bmatrix} [A]_{rr} & [A]_{r\theta} \\ [A]_{\theta r} & [A]_{\theta\theta} \end{bmatrix} \tag{6}$$

$$[B]_{tz} = [B]_{zt}^T = \begin{bmatrix} [B]_{rz} \\ [B]_{\theta z} \end{bmatrix} \tag{7}$$

$$[C]_{tt} = \begin{bmatrix} [C]_{rr} & [0] \\ [0] & [C]_{\theta\theta} \end{bmatrix}. \tag{8}$$

The submatrices of $[A]_{tt}$, $[B]_{tz}$, and $[C]_{tt}$ are defined by

$$[A]_{rr} = 2\pi \sum_e \int_e \left(p_z m^2 \frac{1}{r} \{M\} \{M\}^T dr \right.$$
$$\left. - k_0^2 q_r r \{M\} \{M\}^T \right) dr \tag{9}$$

$$[A]_{r\theta} = [A]_{\theta r}^T = 2\pi \sum_e \int_e \left(p_z m \frac{1}{r} \{M\} \{N\}^T \right.$$
$$\left. + p_z m \{M\} \{N_r\}^T \right) dr \tag{10}$$

$$[A]_{\theta\theta} = 2\pi \sum_e \int_e \left(p_z \frac{1}{r} \{N\} \{N\}^T \right.$$
$$+ p_z \{N\} \{N_r\}^T + p_z \{N_r\} \{N\}^T$$
$$\left. + p_z r \{N_r\} \{N_r\}^T - k_0^2 q_\theta r \{N\} \{N\}^T \right) dr \tag{11}$$

$$[A]_{zz} = 2\pi \sum_e \int_e \left(p_r m^2 \frac{1}{r} \{N\} \{N\}^T \right.$$
$$\left. + p_\theta r \{N_r\} \{N_r\}^T - k_0^2 q_z r \{N\} \{N\}^T \right) dr \tag{12}$$

$$[B]_{rz} = [B]_{zr}^T = 2\pi \sum_e \int_e p_\theta r \{M\} \{N_r\}^T dr \tag{13}$$

$$[B]_{\theta z} = [B]_{z\theta}^T = 2\pi \sum_e \int_e \left(-p_r m \{N\} \{N\}^T\right) dr \tag{14}$$

$$[C]_{rr} = 2\pi \sum_e \int_e p_\theta r \{M\} \{M\}^T dr \tag{15}$$

$$[C]_{\theta\theta} = 2\pi \sum_e \int_e p_r r \{N\} \{N\}^T dr \tag{16}$$

where $\{N_r\}$ indicates $d\{N\}/dr$. In this letter, the Gaussian quadrature is applied to computation of the element integral.

Here, we consider a multi-layered waveguide where waveguide discontinuity lies at $z = z_i$ ($i = 0, 1, \cdots, M - 1$) as shown in Fig. 1(c). The govern equation in this waveguide is obtained by replacing β to $j\partial/\partial z$ in (4).

$$\frac{\partial^2 \{\phi\}_t}{\partial z^2} + [Q] \{\phi\}_t = \{0\}. \tag{17}$$

In homogeneous region, e.g. i-th layer, $z \in (z_{i-1}, z_i)$, the solution of (17) can be written by

$$\{\phi(z)\}_t = \exp\left[-j\sqrt{[Q]_i}(z - z_{i-1})\right] \{\phi\left(z_{i-1}^+\right)\}_t^{\text{F}}$$
$$+ \exp\left[j\sqrt{[Q]_i}(z - z_i)\right] \{\phi\left(z_i^-\right)\}_t^{\text{B}} \tag{18}$$

where $\{\phi\}_t^{\mathrm{F/B}}$ is forward/backward propagating EM wave in z-direction. The propagator in i-th homogeneous region, $[P]_i$, can be derived from (18). The transfer operator at waveguide discontinuity ($z = z_i$), $[T]_i$, can be obtained by continuity condition of transversal EM fields (all components of $\{E\}_t$ or $\{H\}_t$) and power flowing into z-direction (P) [17].

$$\left\{\phi\left(z_i^-\right)\right\}_t^{\mathrm{F}} + \left\{\phi\left(z_i^-\right)\right\}_t^{\mathrm{B}} = \left\{\phi\left(z_i^+\right)\right\}_t^{\mathrm{F}} + \left\{\phi\left(z_i^+\right)\right\}_t^{\mathrm{B}} \quad (19)$$

$$[F]_i\left\{\phi\left(z_i^-\right)\right\}_t^{\mathrm{F}} + [F]_i\left\{\phi\left(z_i^-\right)\right\}_t^{\mathrm{B}}$$
$$= [F]_{i+1}\left\{\phi\left(z_i^+\right)\right\}_t^{\mathrm{F}} + [F]_{i+1}\left\{\phi\left(z_i^+\right)\right\}_t^{\mathrm{B}} \quad (20)$$

where $[F]_i$ is a matrix related to power calculation:

$$P(z) = \frac{jc}{2k_0}\{\phi(z)\}_t^\dagger [F]_i \{\phi(z)\}_t \quad (21)$$

$$[F]_i = \left([C]_{tt,i} - [B]_{tz,i}[A]_{zz,i}^{-1}[B]_{zt,i}\right)\frac{\partial}{\partial z},$$

where c is the speed of light in free space. $\partial/\partial z$ can be replaced by $-j\sqrt{[Q]_i}$ or $j\sqrt{[Q]_i}$ for forward or backward waves, respectively. The reflection and transmission EM fields in the system can be computed by transfer operators $[P]$, $[T]$ as follows:

$$\left\{\begin{array}{c} \{\phi_{\mathrm{out}}\}_t^{\mathrm{F}} \\ \{0\} \end{array}\right\} = [M]\left\{\begin{array}{c} \{\phi_{\mathrm{in}}\}_t^{\mathrm{F}} \\ \{\phi_{\mathrm{in}}\}_t^{\mathrm{B}} \end{array}\right\} \quad (22)$$

$$[M] = [P]_{\mathrm{out}}[T]_{M-1}[P]_{M-1}\cdots[T]_1[P]_1[T]_0[P]_{\mathrm{in}} \quad (23)$$

where $\{\phi_{\mathrm{in}}\}_t^{\mathrm{F}}$ indicates an input field, $\{\phi_{\mathrm{in}}\}_t^{\mathrm{B}}$ and $\{\phi_{\mathrm{out}}\}_t^{\mathrm{F}}$ are reflection and transmission fields, and $[P]_{\mathrm{in/out}}$ is a propagator in the input/output waveguide. The B-Schur [14] is applied to computation of the square root of $[Q]$ at each homogeneous region. To get exponential of matrix, $\exp[-j\sqrt{[Q]_i}(z-z_{i-1})]$ and $\exp[j\sqrt{[Q]_i}(z-z_i)]$, included in (18), we employ Padé approximation with accurately computed $\sqrt{[Q]}$, for details, refer to [10].

The scattering operator, which is preferred in terms of numerical stability, can also be composed by the same manner in [9], [18]. Using doubling procedure of the scattering matrix, large scale periodic waveguides can be analyzed stably as follows:

$$\left\{\begin{array}{c} \{\phi_{\mathrm{in}}\}_t^{\mathrm{B}} \\ \{\phi_{\mathrm{out}}\}_t^{\mathrm{F}} \end{array}\right\} = [S]\left\{\begin{array}{c} \{\phi_{\mathrm{in}}\}_t^{\mathrm{F}} \\ \{0\} \end{array}\right\} \quad (24)$$

$$[S] = [S]_{\mathrm{out}} \star [S]_\Lambda \star \cdots \star [S]_\Lambda \star [S]_{\mathrm{in}} \quad (25)$$

where $\star$ means Redheffer's star product [19], $[S]_{\mathrm{in/out}}$ is the scattering matrix of input/output system, and $[S]_\Lambda$ is that of single period system.

III. NUMERICAL EXAMPLES

For numerical verification of the BiBPM based on Axi-FVFEM, we apply it to analysis of an air-gap of a fibre surrounded by air, and a FBG sensor with plasmonics. First, the axi-symmetric waveguide with a gap shown in the inset of Fig. 2 is analyzed. The refractive indices are $n_1 = 1.45$, $n_2 = 1$, the core radius is $a = 0.5$ μm, and size of
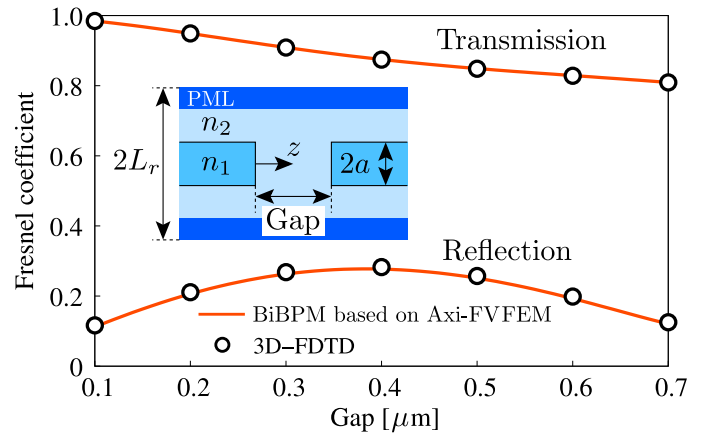

Fig. 2. Fresnel coefficients with respect to length of a gap in an axially symmetric optical waveguide. The inset shows the schematic of the analyzed waveguide.
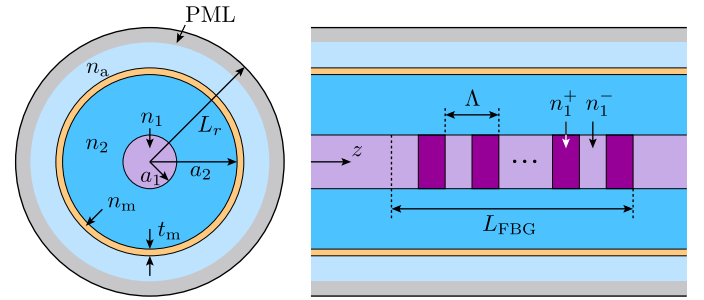

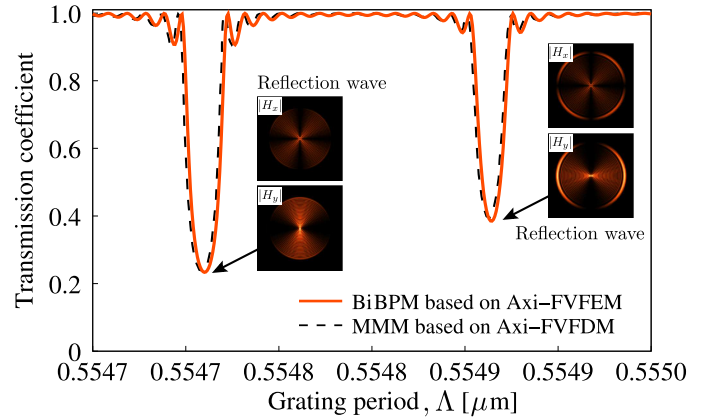Fig. 3. A schematic of a FBG sensor with a metal layer.

Fig. 4. Spectra of transmission coefficients with respect to the grating period. The insets show the magnetic reflection fields.

the computational window including 0.5 μm of the PML is $L_r = 3$ μm which is divided into 35 ringed edge elements. Since refractive index difference is large ($\Delta \approx 26\%$), a sufficiently large number of modes including radiation modes have to be evaluated to compute the Fresnel coefficients accurately. The transfer matrix approach is used to verify $[T]$ and $[P]$ of our formulation, and the results are compared with those of a hand made 3D-FDTD solver. The input wave is let to be HE_{11} wave at wavelength of 1.31 μm, and reflection and transmission coefficients are investigated sweeping the waveguide gap from 0.1 to 0.7 μm. As shown in Fig. 2, the

Fresnel coefficients computed by the BiBPM based on Axi-FVFEM are well in agreement with the results of the 3D-FDTD. In this calculation, run time of one Bi-BPM analysis is about 0.2 seconds using a PC with Intel Xeon CPU X5650 at 2.67 GHz.

Second numerical example is a FBG sensor with a metal layer investigated in [12], where the performance is sensitive to effective index. The schematic of the FBG sensor is shown in Fig. 3. The refractive indices are $n_1^- = 1.446$, $n_1^+ = n_1^- + 0.002$, $n_2 = 1.4356$, $n_\mathrm{m} = 0.3268 \times \delta - j9.7742$, $n_\mathrm{a} = 1.333$. δ is let to be 1×10^{-4} in this analysis. The core radius, thickness of the metal layer, and size of computational window including the 5 μm PML are $a_1 = 4.1$ μm, $a_2 = 36$ μm, $t_\mathrm{m} = 0.036$ μm, $L_r = 60$ μm. The computational window is divided into 250 elements, and HE_{11}^x wave at wavelength of 1.55 μm is launched into the FBG. The length of the FBG is around $L_\mathrm{FBG} = 3$ cm, and transmission coefficients are investigated sweeping the grating period Λ (Duty ratio: 50%) from 0.5547 to 0.555 μm. Since this FBG is periodic and long length, the scattering operator approach is employed to analyze it stably. In this analysis conditions, the run time of one Bi-BPM analysis is about 80 seconds using the same PC in the previous example. Figure 4 shows spectra of transmission coefficients in the FBG sensor, and magnetic reflection fields at $\Lambda = 0.55476$ and 0.5549145 μm are also shown in the insets of the figure. As shown in the insets, the input wave is coupled to a "cladding mode" propagating backward direction at the first dip ($\Lambda = 0.55476$ μm), and a surface plasmon polariton mode at the second dip ($\Lambda = 0.5549145$ μm). The transmission coefficients computed by the BiBPM based on Axi-FVFEM are well in agreement with the results of the MMM with a full-vectorial FD solver reported in [12].

The matrices, such as $[Q]$ and $[S]$, are dense, and matrix inversion is required. However, computational effort of matrix inversion is small because it is substantially 1D problem. In [13], [20], direct FEMs and field-based methods with transfer matrices are compared, and it is pointed out that the computational effort can be less than direct FEMs especially for periodic waveguides. Although there is room for discussion about accuracy, it is difficult to apply direct FEMs to a large scale waveguide as shown in the second numerical example due to computational cost. In addition, we can see that there is no large error which is problem in practical use as shown in numerical examples.

IV. Conclusion

We first present the formulation of the BiBPM based on full-vectorial FEM for axially symmetric waveguides. For numerical validation, an air gap in an axi-symmetric high-index-contrast waveguide and a FBG sensor utilizing plasmonics are analyzed. The results of the present method are well in agreement with those of other numerical modeling.

References

[1] C. E. Rubio-Mercedes, V. F. Rodriguez-Esquerre, A. M. F. Frasson, and H. E. Hernandez-Figueroa, "Novel FEM approach for the analysis of cylindrically symmetric photonic devices," *J. Lightw. Technol.*, vol. 27, no. 21, pp. 4717–4721, Nov. 2009.

[2] D. B. Davidson and R. W. Ziolkowski, "Body-of-revolution finite-difference time-domain modeling of space–time focusing by a three-dimensional lens," *J. Opt. Soc. Am. A*, vol. 11, no. 4, pp. 1471–1490, Apr. 1994.

[3] A. Taflove and S. C. Hagness, *Computational Electrodynamics: The Finite-Difference Time-Domain Method*, 3rd ed. Norwood, MA: Artech House, 2005, ch. 12.

[4] H.-P. Nolting and G. Sztefka, "Eigenmode matching and propagation theory of square meander-type couplers," *IEEE Photon. Technol. Lett.*, vol. 4, no. 12, pp. 1386–1389, Dec. 1992.

[5] J. Mu, H. Zhang, and W.-P. Huang, "Investigation of long-range surface plasmon polaritons gratings by complex mode matching method," *Proc. SPIE*, vol. 6642, pp. 157–164, 2007.

[6] H. Liang, J. Mu, R. A. Soref, X. Li, and W. Huang, "An optical mode-matching method with improved accuracy and efficiency," *IEEE J. Quantum Electron.*, vol. 51, no. 2, pp. 1–8, Feb. 2015.

[7] X. Lu, Z. Cao, M. C. Beurden, Y. Jiao, Q. Wu, and T. Koonen, "A mode-matching method for three-dimensional waveguides with PMLs combined with energy conservation," *J. Lightw. Technol.*, vol. 36, no. 23, pp. 5573–5579, Dec. 2018.

[8] Y.-C. Lu, L. Yang, W.-P. Huang, and S.-S. Jian, "Unified approach for coupling to cladding and radiation modes in fiber Bragg and long-period gratings," *J. Lightw. Technol.*, vol. 27, no. 11, pp. 1461–1468, June 2009.

[9] P. L. Ho and Y. Y. Lu, "A bidirectional beam propagation method for periodic waveguides," *IEEE Photon. Technol. Lett.*, vol. 14, no. 3, pp. 325–327, Mar. 2002.

[10] S. Wu and J. Xiao, "An efficient semivectorial bidirectional beam propagation method for 3-D optical waveguide structures," *J. Lightw. Technol.*, vol. 34, no. 4, pp. 1313–1321, Feb. 2016.

[11] A. M. A. Said, A. M. Heikal, N. F. F. Areed, and S. S. A. Obayya, "Why do field-based methods fail to model plasmonics?," *IEEE Photonics J.*, vol. 8, no. 5, pp. 1–13, art no. 4802613, Oct. 2016.

[12] Y.-C. Lu, W.-P. Huang, and S.-S. Jian, "Influence of mode loss on the feasibility of grating-assisted optical fiber surface plasmon resonance refractive index sensors," *J. Lightw. Technol.*, vol. 27, no. 21, pp. 4804–4808, Nov. 2009.

[13] Y. I. Abdelhak, A. M. Said, N. F. Areed, and S. S. A. Obayya, "Efficient scalar bidirectional beam propagation analysis for photonic devices with circular symmetry," *IEEE Photon. Technol. Lett.*, vol. 33, no. 1, pp. 43–46, Jan. 2021.

[14] E. Deadman, N. J. Higham, and R. Ralha, "Blocked Schur algorithms for computing the matrix square root," in Proc. 11th Int. Conf. Appl. Parallel Scientific Comput., 2013, vol. 7782, pp. 171–182.

[15] F. L. Teixeira and W. C. Chew, "General closed-form PML constitutive tensors to match arbitrary bianisotropic and dispersive linear media," *IEEE Microwave Guided Wave Lett.*, vol. 8, no. 6, pp. 223–225, June 1998.

[16] M. Koshiba, S. Maruyama, and K. Hirayama, "A vector finite element method with the high-order mixed-interpolation-type triangular elements for optical waveguiding problems," *J. Lightw. Technol.*, vol. 12, no. 3, pp. 495–502, Mar. 1994.

[17] K. Morimoto and Y. Tsuji, "Full-vectorial analysis of optical waveguide discontinuities using a propagation operator method based on the finite element scheme," *OSA Continuum*, vol. 2, no. 3, pp. 540–553, Mar. 2019.

[18] A. Iguchi, K. Morimoto, and Y. Tsuji, "Sensitivity-based structural optimal design with bi-directional beam propagation method for photonic devices in high-index-contrast waveguides," *IEEE Photon. J.*, vol. 12, no. 5, pp. 1–11, Oct. 2020.

[19] J. Corones and R. Krueger, "Obtaining scattering kernels using invariant imbedding," *J. Math. Anal. Appl.*, vol. 95, no. 2, pp. 393–415, Sept. 1983.

[20] K. Morimoto, A. Iguchi, and Y. Tsuji, "Novel scattering operator for arbitrary finite element models in optical waveguides," *J. Lightw. Technol.*, accepted for publication.